

Modelling Variability in Full-field Displacement Profiles and Poisson Ratio of Wood in Compression Using Stochastic Neural Networks

Hong Ling, Sandhya Samarasinghe and G.Don Kulasiri

Ling, H., Samarasinghe, S. & Kulasiri, G.D. 2009. Modelling variability in full-field displacement profiles and Poisson ratio of wood in compression using stochastic neural networks. *Silva Fennica* 43(5): 871–887.

Vertical and horizontal displacement profiles in compression parallel-to-grain in a 20×20mm area (30×21 or 630 points) in the Tangential–Longitudinal (T–L) and Radial Longitudinal (R–L) sections of small wood columns were obtained from digital image correlation applied to simultaneously captured images of the two surfaces. These consisted of 21 displacement realisations of 30 points along the length of the specimen. They revealed considerable local variations. Stochastic neural networks were successfully developed to simulate trends and noise across and along a specimen in both displacements as well as Poisson ratios in T–L and R–L sections for two selected load levels of 20kN and 40kN. These networks specifically embed noise characteristics extracted from data to generate realistic displacement and Poisson ratio realisations with inherent variability. Models were successfully validated using independent data extracted based on bootstrapping method with high accuracy with R^2 ranging from 0.79 to 0.91. The models were further validated successfully using a second approach involving Confidence Intervals generated from the data extracted from the models. Models and experimental results revealed that for 20kN load, both vertical and horizontal displacements in T–L section were less heterogeneous across the specimen (smaller vertical shearing and horizontal strain, respectively) than those in the R–L section. For the 40kN load, both displacement profiles in the T–L section were less noisy and more compact than those for the 20kN load indicating less heterogeneity due to compaction of structure. In the R–L section, larger vertical shearing and horizontal strains persisted at 40 kN load. Poisson ratio decreased with load and it was nonlinear in both sections but T–L section showed much less noise across the specimen than the R–L section.

Keywords wood, displacement profiles, variability, digital image correlation, micro-structure, stochastic neural networks, Poisson ratio

Addresses Centre for Advanced Computational Solutions (C-fACS), Lincoln University, Canterbury, New Zealand **E-mail** Sandhya.Samarasinghe@lincoln.ac.nz

Received 1 September 2008 **Revised** 14 April 2009 **Accepted** 28 August 2009

Available at <http://www.metla.fi/silvafennica/full/sf43/sf435871.pdf>

List of Symbols

Symbol	Definition
u	vertical displacement
v	horizontal displacement
AI	Approximate Identity
AINN	Approximate Identity Neural Network
AINNs	Approximate Identity Neural Networks
ANNs	Artificial Neural Networks
CI	Confidence Interval
COV	Covariance
DIC	Digital Image Correlation
KL	Karhunen-Loève
MLP	Multilayer Perceptron
MPM	Material Point Method
NN	Neural Network
RBF	Radial Basis Function
R-L	Radial-Longitudinal
SEM	Scanning Electron Micrograph
SNN	Stochastic Neural Network
SNNs	Stochastic Neural Networks
T-L	Tangential-Longitudinal
ν	Poisson ratio
WN	White Noise

1 Introduction

Presently, analysis of the behaviour of wood is based on the theories and assumptions for homogeneous isotropic or orthotropic materials. However, wood is a highly variable heterogeneous material and the effect of such variable structure on mechanical properties is well recognised. Due to lack of appropriate instrumentation and analytical methods, detailed studies of structural influence on mechanical behaviour of wood are very limited. Recently digital image correlation, a non-contacting full-field displacement analysis technique, has become a useful tool for obtaining full field displacement and strain profiles in materials including wood. The method has been successfully applied to determine displacements of wood in tension and compression and crack-tip displacement fields in wood (Samarasinghe and Kulasiri 2000a, b, 2004). Several investigators have applied it to study compression behaviour of small wood specimens (Zink et al. 1995, Choi et

al. 1991, 1996) and bolted wood joints (Stelmokas et al. 1997). In this investigation, digital image correlation is used to obtain full field displacement profiles in compression and model these profiles using a novel neural network method, stochastic neural networks, that can capture noise inherent in a system. These models will allow full characterisation of the influence of the variability in the heterogeneous anatomical structure on wood properties.

1.1 Objectives

The goal of this research is to model full field displacement profiles in wood in compression using advanced neural networks based on experimental data collected from digital image correlation (DIC) method. Specifically, a) full field displacement profiles are studied in compression parallel-to-grain simultaneously in Tangential-Longitudinal (T-L) and Radial-Longitudinal (R-L) sections in order to conduct a detailed assessment of the nature of the displacement characteristics in these sections and relate them to the typical microstructure of T-L and R-L sections, and b) stochastic neural networks are developed to model the variability or noise characteristics found in the displacement profiles at different load levels as well as to study and model localised Poisson ratio variations in T-L and R-L sections in compression.

2 Background

Samarasinghe and Kulasiri (2000a, b, 2004, Samarasinghe et al. 2007) successfully used digital imaging in the studies of wood displacement to characterise various aspects of wood behaviour including displacement parallel- as well as perpendicular-to-grain in tension, crack-tip displacements, and displacement in wood beams. They specifically revealed the highly variable nature of the displacement profiles obtained from the images analysed by the Digital Image Correlation (DIC) method. Samarasinghe and Kulasiri (2000a) related the full-field displacements in tension-parallel-to grain to the underlying cel-

lular structure. They pointed out that when the tracheids carry the load in parallel-to-grain tension, a substantially complex and noisy displacement patterns result whereas the corresponding perpendicular-to-grain displacement profiles are much smoother, similar to that of isotropic rubber, which they stated could be an indication of the properties of lignin that binds the cells together.

Choi et al. (1991) studied parallel-to-grain compression behaviour of very small wood samples of $1 \times 1 \times 4$ mm and tensile behaviour of very small paperboard samples of 5×20 mm. For wood, they obtained strain parallel- and perpendicular- to loading in an area of 0.63×2.58 mm for several load levels. The most notable feature of their strain profiles was that there was a considerable variation in strain throughout the area analysed for a constant load level. For example, strain in the load direction varied from 0.76% to -1.0% where positive values indicate tension and negative values indicate compression showing that some areas within a compression specimen undergo tension in the direction of load. Strain perpendicular-to-loading also showed high variation ranging from -1.26% to 1.12% for a constant load level, where positive and negative values indicate tension and compression, respectively. Such variations indicate a significant influence of wood structure on strain fields in small specimens. For paperboard, there was variation in strain but the scatter was much less compared to wood. In a paper published later in 1996, Choi et al. graphically presented contours of these highly variable strains for wood and showed that strains become concentrated near rays closer to the edge of a compression specimen. With further increase in loading, these areas of strain concentration become large resulting in a failure zone associated with an area around a ray. The authors stated that failure was due to stress concentrations near rays and buckling of fibres associated with these rays.

Zink et al. (1995) showed a similar phenomenon to that described above for larger wood specimens under compression parallel-to-grain loading. They compared strains in aluminium and wood blocks of dimensions $25.4 \times 25.4 \times 101.6$ mm tested in compression. They found very uniform strains throughout the surface of aluminium but highly variable strains in wood. For example,

range of strain for aluminium for a particular load was 1800–2000 μ strain, whereas for wood, strain varied within a much broader range between 1250–2950 μ strain. They also found that the strain in wood varied along the length as well as across the specimen. Another interesting observation was that in some areas strain perpendicular to load was greater than that in the direction of load, which raises serious questions about the accepted notion of Poisson ratio. Zink et al. (1995) further state that the local areas of strain concentrations develop at load levels even below the proportional limit confirming the similar observations made for much smaller specimens by Choi et al. (1991, 1996).

Nairn (2006) modelled transverse compression in one growth ring based on a scanning electron micrograph (SEM) image of wood, which he converted to material points in a grid based on the image intensity variation that reflects density variation in the cellular structure. He analysed it using material point method (MPM) for the cases of elastic and elastic-plastic behaviour with cellular properties obtained from literature. He demonstrated various aspects of deformation and collapse of cellular structure, which in general agreed with observed behaviour reported in literature. He reported the stress-strain relationship of the specimen as a whole. To date however, no work has been done to explicitly model the variability in localised wood behaviour. In our study, simultaneous full field displacement measurements in the T-L and R-L sections are obtained in compression parallel-to-grain. These are reviewed closely to understand patterns and relate them to typical microstructure in these sections. The displacement profiles are then used in the development of an advanced neural network, a stochastic neural network, that can capture intrinsic noise in a specimen to model localised variation in displacements and Poisson ratios in the two sections.

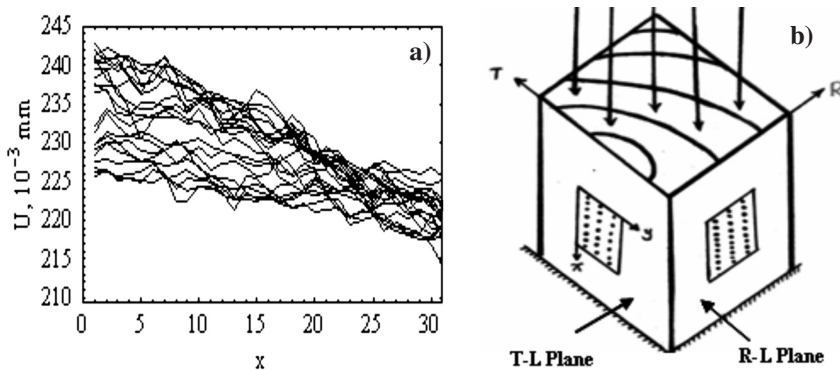


Fig. 1 (a) Experimentally obtained vertical displacement profiles in the T–L section. (Horizontal axis, x , indicates the location of 30 points (shown along x axis in Fig. 1b) where displacements were measured: the distance between two adjacent points is 10 pixels; scale: 14.6 pixels/mm); (b) Specimen configuration showing simultaneous camera view of the T–L and R–L planes and location of the areas (rectangular blocks with dots) subsequently analysed in the two sections.

3 Methods

There are two aspects to the study: 1) experimental programme to simultaneously capture images of the T–L and R–L sections of wood specimens and analyse the images for determining full field displacement fields in compression; and 2) developing stochastic neural networks for modelling wood displacements and Poisson ratio characterised by variability. These two aspects are addressed in this section.

3.1 Experimental Method: Digital Image Processing

Experiments were conducted on small wood columns (44×44mm cross section and 136 mm height parallel-to-grain) cut from clear kiln-dried *Pinus radiata* (radiata pine). The average moisture content of the specimens at the time of testing was 15.1% and dry specific gravity was 0.46. Before testing, two T–L and R–L sections of specimens were sprayed with black paint to prepare the surface for obtaining good quality images suitable for analysis with Digital Image Correlation (DIC). The test procedure was that of a standard compression test. A specimen was placed on the testing platform of a SINTECH/MTS 30-D computer controlled testing machine

in such a way that the two T–L and R–L surfaces were in view of the camera (Fig. 1b). An Ikegami CCD camera with 25 frames a second capture rate was used and images were digitised to 512×512 pixels by a high accuracy CX100 frame grabber. As both T–L and R–L sections of a specimen were captured simultaneously into one image, an image consists of two symmetrically placed images of the T–L and R–L surfaces. Priori to testing, a graph paper was placed against the two sides and their images were captured to convert the pixels to mm and the scale thus found was 14.6 pixels/mm for T–L section and 14.4 pixels/mm for the R–L section. (In the subsequent image analysis, the scales were adjusted to account for the fact that the wood surfaces are inclined 45° to the image plane). The graph paper was removed and an image of the specimen before loading was captured and then it was loaded at a rate of 2 mm/min. Images were captured at various load levels up to failure and stored for processing with Digital Image Correlation (DIC).

DIC compares the original undisplaced images with images after displacement using a pattern matching algorithm that follows the movement of a local neighbourhood of points from the undisplaced to the displaced images. Greater details of the method can be found in various publications (Samarasinghe and Kulasiri 2000a, b, 2004). In this study, a 20×20 mm² area in each of the

images of T–L and R–L sections (Fig.1b) was analysed in order to fully appreciate the minute local details of the displacement profiles. From the DIC method, vertical and horizontal displacements of 630 points corresponding to 30 rows and 21 columns in each section were obtained. In order to aid the discussion on fundamentals of stochastic neural network development that will be presented in the next section, the vertical displacements (u) in the T–L section of a specimen are illustrated in Fig. 1a. One line graph in this figure is called a displacement realisation and represents displacements along one vertical column of 30 points in the analysed area in the T–L section (Fig. 1b which also shows the coordinate system (x, y) used). There are 21 such realisations in Fig.1a corresponding to the 21 columns of 30 points. Ideally, these realisations should be identical without noise for perfect material homogeneity. As the figure reveals, there is substantial noise in the displacements as a result of the variability in the underlying heterogeneous wood structure. It is proposed to model this variability using stochastic neural networks that is based on the theory of stochastic processes.

3.2 Analytical Methods: Stochastic Neural Networks

Artificial Neural Networks (ANNs) are an approach that models complex natural and biological systems on the basis of mimicking the information processing methods in the human brain. ANNs have high capability in approximating input-output mappings that are complex and nonlinear to arbitrary degree of precision (Samarasinghe 2006). These capabilities of neural networks make them suitable to address some of the problems related to stochastic processes that are characterised by noise. Stochastic Neural Networks (SNNs) are a kind of ANN that captures the variability inherent in a system while following trends in the system behaviour. This makes it suitable for analysing noisy behaviour of wood due to natural variation of anatomical properties and microscopic defects.

In this context, a stochastic process may be regarded as a set of values obtained from an experiment to observe the spatial development of

a stochastic variable which does not have a unique value for the corresponding spatial coordinate x . This means that a different set of observations can be obtained when repeating the same experiment such as the 21 displacement realisations obtained for the same wood specimen as shown in Fig. 1a. Mathematically, a stochastic process is a collection of random variables over the time or space parameter x ($x \in X$) and the complex stochastic process is represented by the sum of elementary stochastic functions (Turchetti 2004); specifically, by a linear combination of non-random (deterministic) functions and zero-mean random variables. For many complex natural and biological processes, these non-random (deterministic) functions are not known a-priori and must be estimated from data. In this case, Karhunen-Loève (KL) theorem plays a central role in representing an observed stochastic process (Turchetti 2004).

In KL representation, a stochastic process is viewed as a bundle of finite number of realizations (such as the 21 displacement realisations) from a real stochastic processes collected over a finite number of points (such as the 30 points in Fig. 1a). Outcomes at a particular point x is considered a random variable. For instance, in the case of wood displacements in Fig. 1a, there are 30 random variables corresponding to displacements at the 30 points along a vertical line. Each variable has 21 values. In a stochastic process, these random variables are generally correlated and the covariance (COV) matrix depicts these relationships.

Now let us consider a stochastic process $\xi(x)$ and its covariance matrix. The KL expansion represents a stochastic process as a linear combination of a finite number of orthogonal functions determined by the covariance matrix (Gilman and Skorohod 1974). Thus a stochastic process can be expanded as the following Eq. 1 associated with the COV given in Eq. 2.

$$\xi(x) = \sum_{j=1}^n \phi_j(x) \zeta(\lambda_j) \quad (1)$$

$$COV(x_1, x_2) = \sum_{j=1}^n \lambda_j \phi_j(x_1) \phi_j(x_2) \quad (2)$$

where $\xi(\lambda)$ is an orthogonal sequence of random variables with zero-mean and variance equal to the eigenvalues (λ) of the covariance matrix of

the stochastic process, $\phi(x)$ are the eigenfunctions corresponding to the eigenvectors in the covariance matrix, and x_1 and x_2 are any two spatial locations in the domain of x . The two items, $\xi(\lambda)$ and $\phi(x)$, need to be estimated to complete the model in Eq. 1. In the KL expansion, COV matrix is decomposed into a set of eigenvectors and eigenvalues. Eigenvectors denote independent orthogonal directions relevant to the data and eigenvalues represent the portion of variability in the original data captured by them. There are as many eigenvectors as there are random variables (i.e. discrete spatial points). This decomposition of COV matrix is called the eigenvalue decomposition and it produces a new coordinate system, depicted by eigenvectors, where variables are independent and therefore, the COV between any two new variables is zero. Variance of each new variable is denoted by the corresponding eigenvalue.

The eigenfunctions $\phi(x)$ needed to construct the stochastic function in Eq. 1 are the functions fitted to each of the eigenvectors. This basically converts discrete points of an eigenvector into an eigenfunction. Since $\phi(x)$ are deterministic functions, they can be modeled by deterministic neural networks. For these networks, input is x and output is the corresponding eigenvector. The $\xi(\lambda)$ is a random variable with zero-mean and λ variance and has the same attributes as the so called White Noise, a discrete stochastic process represented by a Gaussian distribution with zero-mean and variance σ^2 which in this case is equal to the eigenvalue λ of each of the eigenvectors. The $\phi(x)$ can then be linearly combined with White Noise $\xi(\lambda)$ as in Eq. 1 to develop a stochastic neural network as shown in Fig. 2.

Thus the whole stochastic process can be regarded as a linear combination of the product of the independent eigenfunctions $\phi(x)$ and their corresponding White Noise (WN) $\xi(\lambda)$. In Fig. 2, $\xi(x)$ is the mean of the stochastic process at point x .

Developing a stochastic neural network thus involves two aspects: generating deterministic eigenfunctions $\phi(x)$ and White Noise $\xi(\lambda)$ from measured data (e.g. displacement data). To model eigenfunctions, eigenvectors need to be first determined by calculating the COV from measured data and decomposing it using KL expansion.

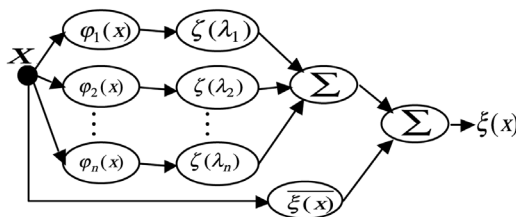


Fig. 2. The structure of the Stochastic Neural Network (SNN).

This results in eigenvectors and corresponding eigenvalues from which significant eigenvectors are determined. From each significant eigenvector, eigenfunction is modelled using deterministic neural networks. The corresponding $\xi(\lambda)$ is generated by means of Gaussian distributions with 0 mean and variance λ associated with that $\phi(x)$. These $\phi(x)$ and $\xi(\lambda)$ are linearly combined as in Fig. 2 to complete the SNN. This network will produce a different displacement realisation each time it is run in a way that preserves the COV of the data. The next section presents the development of deterministic neural networks for simulating eigenfunctions from the corresponding eigenvectors.

3.2.1 Developing Deterministic Neural Networks

Input to each of the deterministic NN representing one eigenfunction is the coordinate x and output is the corresponding component of the eigenvector being modeled. Generation of the eigenvectors is described in this section using the data shown in Fig. 1 as an example. The dataset is a bundle of realisations of a stochastic process $\xi(x)$ ($u(x)$ in this example). Assume that $\xi^k(x)$ denotes the k^{th} realisation. For each realisation, there are n different values corresponding to n discrete points (30 points in the example). The COV of this stochastic process describes the relationship between values of all realisations at any two discrete points. If we assume that $\xi(x)$ at each discrete point x is viewed as one variable, then the value of each realisation $\xi^k(x)$ at each discrete point x will be viewed as an instance of the corresponding variable. So we denote the whole

group of variables on the dataset by vector $\xi(x) = \{ \xi(x_1), \xi(x_2), \dots, \xi(x_n) \}$ where $\xi(x_i)$ contains all values of realisations at the i^{th} discrete point x_i i.e., $\xi(x_i) = \{ \xi^1(x_i), \xi^2(x_i), \dots, \xi^k(x_i) \}$. In this vector representation, the mean and variance of all realisations at a particular discrete point x_i and the covariance of all realisations between any two different discrete points x_i and x_j can be efficiently calculated by using the following equations (Samarasinghe 2006):

$$\overline{\xi(x)} = \frac{1}{K} \sum_{k=1}^K \xi^k(x) \tag{3}$$

$$COV = \frac{1}{K-1} \sum_{k=1}^K (\xi^k(x) - \overline{\xi(x)}) (\xi^k(x) - \overline{\xi(x)})^T \tag{4}$$

In Eq. 3, $\overline{\xi(x)} = \{ \overline{\xi(x_1)}, \overline{\xi(x_2)}, \overline{\xi(x_3)}, \dots, \overline{\xi(x_n)} \}$ is a vector which contains all mean or expected values of realisations at each discrete point x_i and k is the number of realisations in the dataset (21 in this example). In Eq. 4, COV is the covariance matrix which contains all variances and covariances. COV is a symmetric matrix with size $n \times n$ where n is the number of discrete points. The diagonal entries of COV represent variances and off-diagonal entries represent covariances between any two different discrete points. Once the COV is constructed, eigenvalues and eigenvectors of the COV matrix can be extracted from mathematical or statistical software.

The model development involves firstly, the creation of a number of deterministic neural networks to simulate the significant eigenfunctions $\phi_j(x)$ of the COV matrix. The number of significant eigenfunctions is decided by the number of eigenvalues that play a significant role in the KL representation of these realisations. Each significant eigenfunction is modelled by a neural network where input is x and output is the corresponding eigenvector.

There are three main deterministic neural networks for function approximation: Multilayer Perceptron (MLP) Networks (Samarasinghe 2006), Radial Basis Function (RBF) Networks (Park and Sandberg 1991) and Approximate Identity Neural Networks (AINN) (Turchetti 2004). All of them have powerful capability in approximating arbitrary deterministic input-output mappings. In this study, a series of Approximate Identity Neural

Networks (AINNs) is developed to represent the significant eigenfunctions $\phi_j(x)$.

In modelling Artificial Neural Networks (ANN), important factors are: the number of neurons, the structure of network and the learning algorithm. The number of neurons depends on the complexity of the input-output mapping. This study employs an AINN with one input and one output and one hidden layer with Approximate Identity (AI) function

$$\omega(x) = \tanh\left(\frac{v(x - \vartheta) + \sigma}{2}\right) - \tanh\left(\frac{v(x - \vartheta) - \sigma}{2}\right)$$

as the activation function, where v defines the sharpness of the function, ϑ defines the centre of symmetry and σ defines the position of the maximum of the function. This function has the form of Gaussian distribution with some special properties (Truchetti 2004). The backpropagation algorithm was used to minimize the network's global error between the actual network outputs and their corresponding desired outputs.

Trained deterministic neural networks contain the weights and parameters of the stochastic neural network. Then stochastic properties of the network are achieved by adding the corresponding WN ($\xi(\lambda)$) processes to each of the deterministic neural networks as shown in Fig. 2. The next section applies SNN to wood data, validates the model and analyses the results.

4 Results and Discussion

Fig. 3 depicts the coordinate system and the area analysed on the wood surface. The x axis lies along the direction of the compression load and y axis is perpendicular to the load. Further processing and plotting of experimental displacement profiles as well as SNN developments were done on Mathematica 5.2 (Wolfram Research 2005).

4.1 Cell Structure of Wood

Before discussing the structural influence on mechanical behaviour of wood, it is necessary to closely look at T-L and R-L sections in terms of their anatomical features. Wood (*Pinus radiata*)

consists largely of vertical tracheids which run longitudinally through the wood in the vertical axis of the trunk. Ray cells run horizontally through the wood in the radial direction of the trunk throughout its height (Jane 1956). These two predominant types of cells are organised into a composite structure as shown in Fig. 4 for R–L

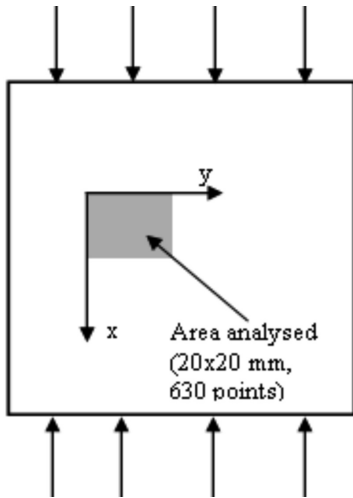


Fig. 3. Coordinate system and location of analyzed area on the wood surface.

and T–L sections. In this study, focus is to assess the structural influence of these two types of surface on displacements and model this behaviour characterised by noise.

In the R–L section (Fig. 4a), the white columns are the radial walls of the vertical tracheids and there are three sheets of ray in the horizontal direction. The small white circles are pits that are the communication channels between cells. In the T–L section (Fig. 4b), the white vertical columns are the tangential walls of the vertical tracheids organised around the cross section of piles of rays. As the natural structure of wood is quite different in these two longitudinal sections, the arrangement of the cells is expected to affect the mechanical behaviour of wood. For this reason, this study individually analyses the two sections to study the structural influence of wood on the displacement patterns and corresponding Poisson ratios when loaded in compression. A unique feature of the study is that the analysis is made on the same specimen using simultaneously captured images of the two surfaces.

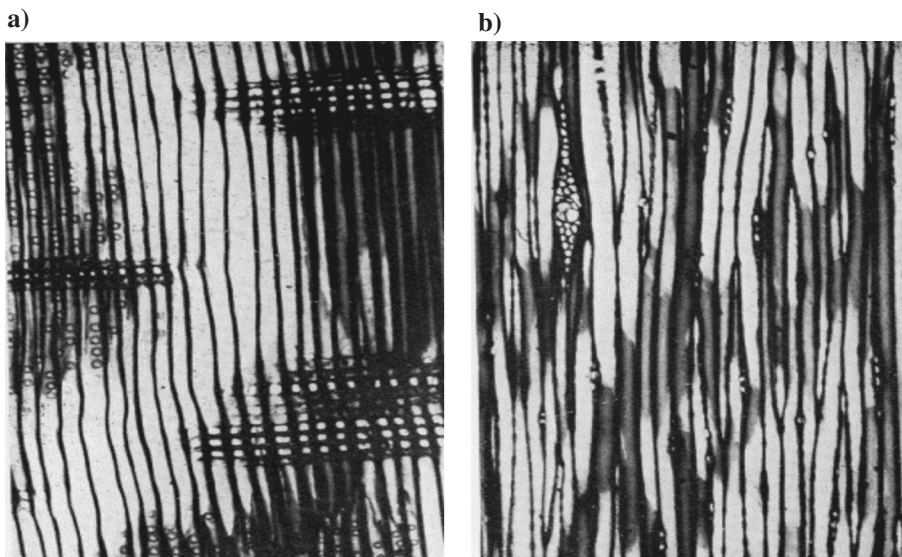


Fig. 4. The anatomical cell structure of softwood: (a) R–L section and (b) T–L section (Jane 1956).

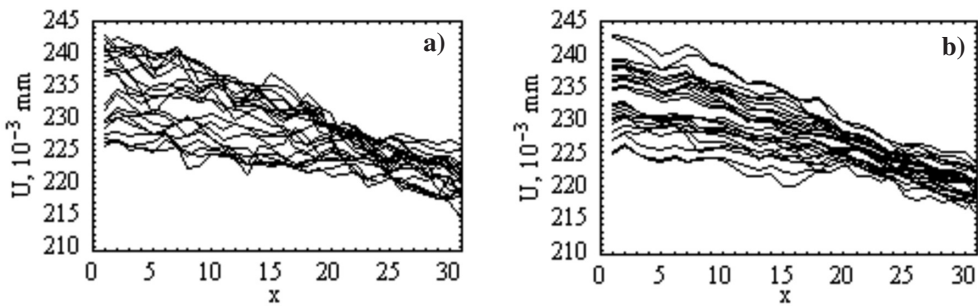


Fig. 5. Vertical displacement profiles in the T-L section under 20kN compression load. (a) experimental data and (b) predictions from the developed stochastic neural network. (Horizontal axis, x , depicts the location of 30 points (10 pixels apart), where displacements were measured (see Fig. 1b). scale: 14.6 pixels/mm).

4.2 Displacement Realisations in the T-L Section (20kN)

4.2.1 Vertical Displacement (u)

The vertical displacement is that in the direction of x -axis in the coordinate system shown in Fig. 3. When loaded in compression parallel-to-grain, vertical displacement (u) measures the amount of contraction in the same direction as the load. In this direction, load is taken by the longitudinal tracheids (Fig. 4b) that can undergo compression as well as longitudinal shear and buckling. Rays act as discontinuities to load flow. This is expected to produce non-uniform characteristics in displacements. Fig. 5a presents the vertical displacement (u) obtained for a specimen from images using the DIC method for a 20kN load and each realisation is a series of displacement measurements at 30 points along one vertical column in the image. There are 21 such realisations here representing displacement along 21 such columns of 30 points. The vertical displacement (u) randomly ranges from 0.22 mm and 0.25 mm for the constant load of 20kN. All vertical displacement realisations are quite different from each other and the changes in a particular realisation are complex and stochastic. Thus, there are two aspects to noise or variability in this figure: one aspect is the noise in each realisation denoting the effect of variability along the length and the other is the difference between any two realisations denoting the effect of variability of structure across the specimen. In this paper, the

first term is called noise along the grain or length and the latter is termed noise across the specimen due to relative displacement (longitudinal shear) between two adjacent columns of points. Referring to Fig. 4b, sources of noise along the grain depicted in one realisation appear to be randomly distributed stacks of rays that are encountered by the load carrying tracheids and the variability of tracheids themselves that undergo compression, shear and buckling. As for the difference between realisations, they indicate that longitudinal shearing has taken place. This can be between tracheids and/or between rays and tracheids and can be assisted by lignin. Fig. 5a shows that there is noticeable noise in both directions. Fig. 6a presents the covariance matrix of all vertical displacement (u) profiles.

In order to develop a stochastic neural network, COV matrix of these vertical displacement profiles were generated and decomposed using KL expansion as described previously. The number of significant eigenvalues and their corresponding eigenvectors were extracted from the distribution of eigenvalues (Fig. 7). There are three significant eigenvalues and therefore, three different AINNs were developed for simulating the three corresponding eigenfunctions. The first eigenvalue amounts to 93% indicating that most of the data variation is captured by the first eigenvector; the other two eigenvectors capture 1.47% and 1.18% of variance, respectively.

All AINNs representing significant eigenfunctions have the same structure but have different number of neurons and values of network param-

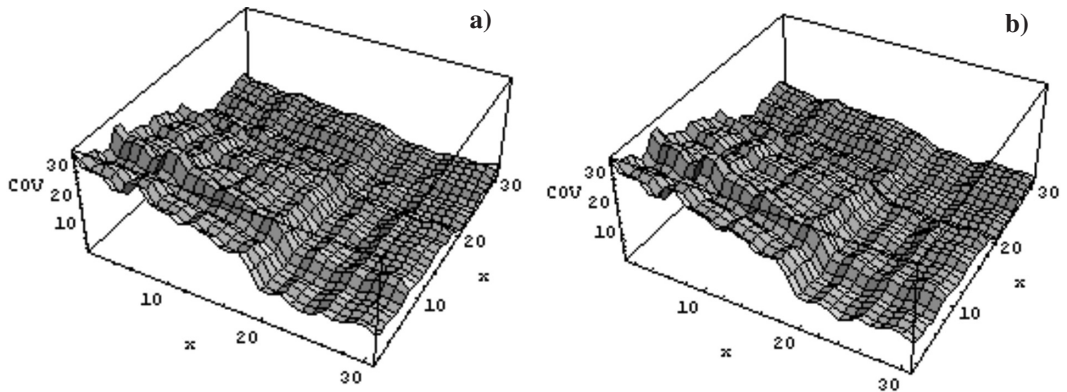


Fig. 6. The covariance matrix of vertical displacement profile in the T–L section under 20kN compression load: (a) experimental data and (b) predictions from the developed stochastic neural network. (Horizontal axis, x , depicts the location of 30 points (10 pixels apart), where displacements were measured. scale: 14.6 pixels/mm).

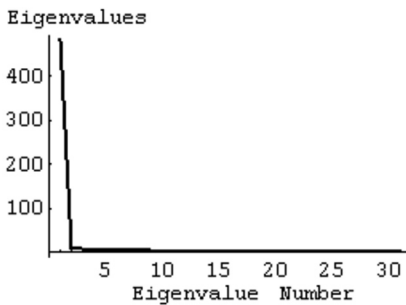


Fig. 7. The distribution of eigenvalues from KL expansion.

eters. Three networks were developed to simulate the three eigenfunctions and Fig. 8 shows the actual data (3 eigenvectors) superimposed on the eigenfunctions $\phi(x)$ approximated by AINN. In the figure, the dots represent eigenvector values while the black lines represent approximated output $\phi(x)$ from the networks. Furthermore, the three AINNs have approximated eigenfunctions with high accuracy (R^2 of each AINN ranges from 0.992 to 0.998). The AINNs were assembled into a stochastic neural network as shown in Fig. 2. The SNN consists of a linear combination of AINNs and corresponding WN ($\xi(\lambda)$) added to the mean displacement values at each discrete point x . Each $\xi(\lambda)$ has zero mean and variance equal to the corresponding eigenvalue. The output of the SNN is one vertical displacement realisa-

tion. From the SNN, as many vertical displacement realisations as desired can be generated and Fig. 5b displays a set of such realisations.

Fig. 5b shows that the vertical displacement realisations from the SNN follow the general behaviour of the vertical displacement observed in experimental data. These outputs of the SNN represent some probable realisations representing the statistical properties of the heterogeneous structure. Therefore, they also can represent the behaviour in other typical areas of the same wood not measured in the experiment.

The covariance matrix of the approximated vertical displacement (u) obtained from 200 realisations from the SNN was used to assess the accuracy of the SNN for simulating vertical compression displacement (u) in wood. Fig. 6b shows the covariance matrix of the approximated u and it resembles the original COV from data extremely well. In order to compare the actual and predicted covariance matrices, the corresponding entries in the two matrices were compared and results are shown in Fig. 9 which indicates a strong linear relationship between the predicted and the actual covariance matrices with an R^2 value of 0.998. Furthermore, the mean square error (MSE) based on the comparison of two COV matrices was 0.0792. This shows that the predicted SNN can simulate vertical displacements in wood well.

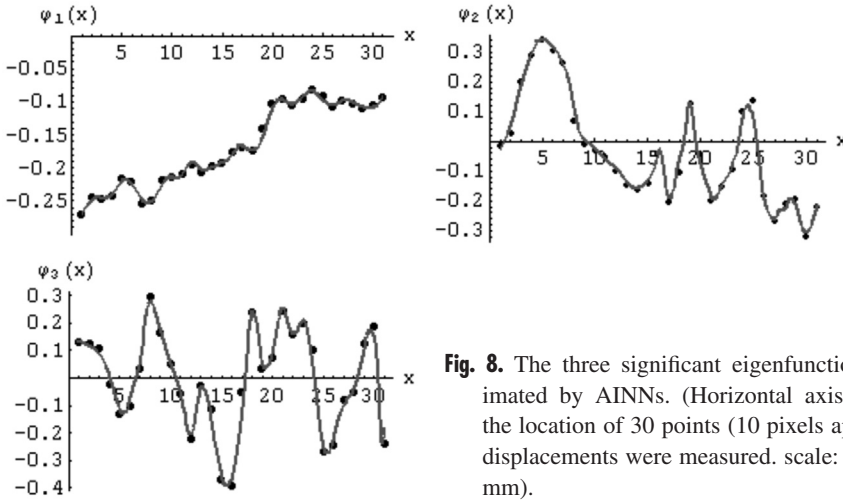


Fig. 8. The three significant eigenfunctions approximated by AINNs. (Horizontal axis, x , depicts the location of 30 points (10 pixels apart), where displacements were measured. scale: 14.6 pixels/mm).

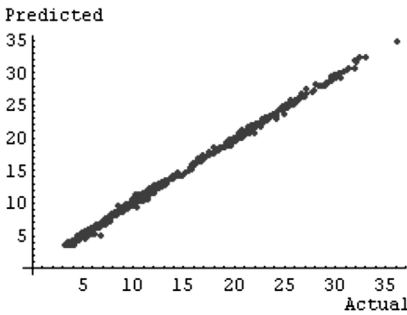


Fig. 9. The linear relationship between the actual and predicted covariance matrices.

4.2.2 SNN Model Validation

Two other methods were applied to confirm the validity of the SNN. One is the traditional validation method for deterministic neural networks – which is to develop the model on a portion (about 70%) of data (training) and use the rest of the data (test data) to validate it. In this study, two independent data sets (not used in developing SNNs) were used to validate the SNN. Specifically, bootstrapping method was employed with two random extractions where each extraction involved partitioning the dataset into 70% samples for training and 30% for testing, developing an SNN using the training data and validating with the test data.

This was repeated for the second random data extraction. (SNN model results presented previously correspond to training data in extraction 1). Fig. 10 presents the relationship between the COV obtained from the SNN generated realisations and COV for experimental realisations for the two test datasets. It indicates a strong linear relationship with R^2 of 0.91 and 0.90, respectively, for the two test datasets.

The other validation method is based on the 95% confidence interval (CI) generated from the SNN based displacement realisations. Here, a large number of realisations (200 in this study) generated from the SNN were used to develop CI using the standard inferential statistical procedures. Then data for two new validation specimens (not used in the previous modelling or testing) were projected onto the CI. If most of these fall within the bounds of the confidence interval, the SNN characterises the generic behaviour of wood. Fig. 11 displays results for the two independent validation specimens and it reveals that most of the realisations are within the CI (2 bold solid lines) indicating that the SNN has captured the essential noise characteristics in wood. Therefore, the developed SNN is capable of simulating trends and noise in wood displacement.

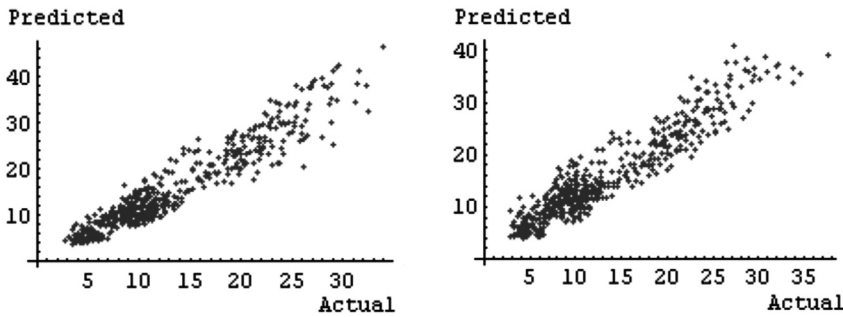


Fig. 10. Linear relationship between the predicted and experimental COV for two different test datasets.

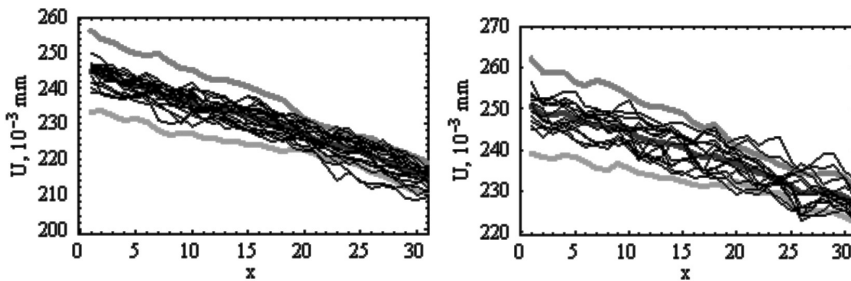


Fig. 11. Validation of SNN using two independent validation specimens based on 95% confidence interval for the displacement realisations extracted from SNN. (Horizontal axis, x , depicts the location of 30 points (10 pixels apart), where displacements were measured. scale: 14.6 pixels/mm).

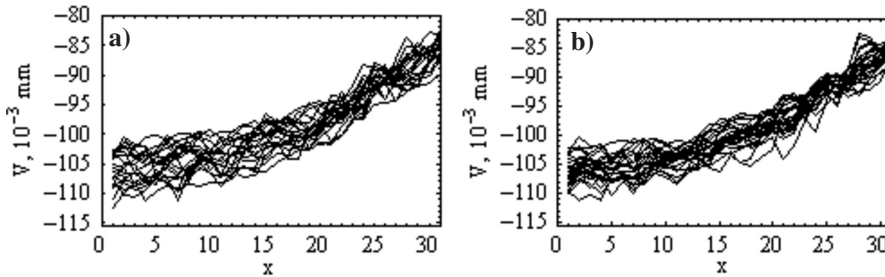


Fig. 12. Horizontal displacement profiles in the T–L section under 20kN compression load: (a) experimental data and (b) predictions from the developed SNN. (Horizontal axis, x , depicts the location of 30 points (10 pixels apart), where displacements were measured. scale: 14.6 pixels/mm). Negative displacements indicate compression.

4.2.3 Horizontal Displacement (v) (T–L Section, 20kN)

The horizontal displacement is that in the direction of y -axis in the coordinate system shown in Fig. 3. When loaded parallel-to-grain, horizontal displacement (v) is a measure of the amount of

displacement in the perpendicular direction to load. As the specimen is loaded in compression, it is expected to undergo expansion in the direction opposite to load. Fig. 12a presents the horizontal displacement (v) obtained for the same area in which u was measured previously.

In Fig. 12a, one profile or realisation is horizon-

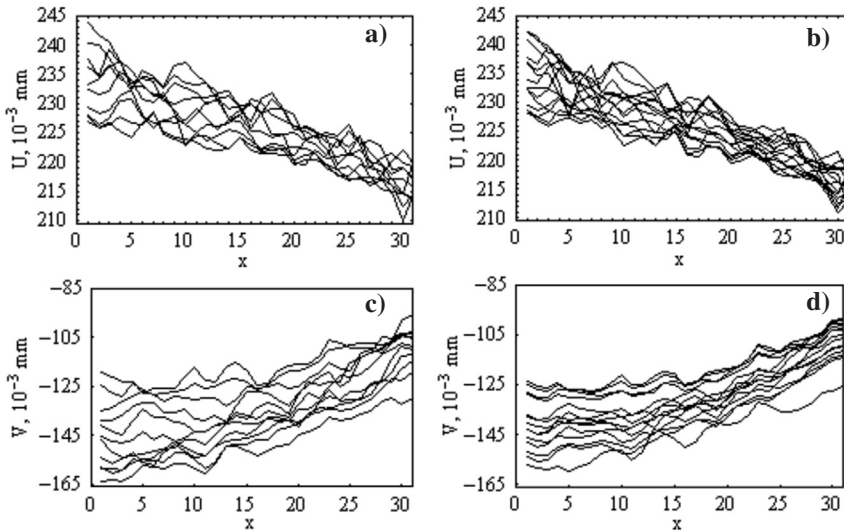


Fig. 13. Comparison of vertical and horizontal experimental displacement realisations with model predictions for R–L section under 20kN compression load: (a) and (c) experimental data for vertical and horizontal displacements; (b) and (d) model predictions. (Horizontal axis, x , depicts the location of points where displacements were measured. scale: 14.4 pixels/mm).

tal displacement along one column of 30 points in the image and there are 21 such realisations. In an ideal homogeneous material, all these profiles would have little or no noise. However, according to Fig. 12a, v is nonlinear and randomly ranges from -0.115 mm to -0.08 mm for a constant load of 20 kN, where negative values indicate compression. Comparing Fig. 12a and Fig. 5a, the influence of loading parallel-to-grain on horizontal displacement is more complex and noisier than that on the vertical displacement. In this mode, randomly distributed stacks of rays (Fig. 4b) may act as stress raisers and may be contributing to the variability and nonlinearity in individual displacement profiles. Notable effect is that the displacement realisations are more compact (closer together) than in the vertical displacement case indicating reasonably uniform horizontal movement of the 21 vertical lines. The difference between two realisations indicates the relative displacement (horizontal strain). Contribution to horizontal displacement in the T–L section in general comes from pits between tracheids and pits between tracheids and rays. Samarasinghe and Kulasiri (2000a) demonstrated that displacement across the grain of a wood specimen loaded

parallel to grain in tension can be as uniform as that of isotropic rubber.

In this case, there are 8 significant eigenvalues which is 5 significant eigenvalues more than those required for the vertical displacement indicating that the individual horizontal displacement realisations have more noise and variance. Eight deterministic neural networks were developed successfully to simulate the 8 corresponding significant eigenfunctions and the resulting models had very high accuracy with R^2 ranging from 0.991 to 0.997. White Noise was then added to each network to develop the SNN. The corresponding actual and predicted COV matrices revealed a strong linear relationship with an R^2 value of 0.983 and MSE of 0.083. Fig. 12b shows some predicted horizontal displacement realisations from the SNN. It compares extremely well with Fig. 12a. The model was validated using the two approaches presented in the previous section. The R^2 for both independent test datasets from bootstrapping was 0.81, and data for the two independent validation specimens were within the respective CI bounds (not shown).

4.3 Displacement Realisations in the R–L Section (20kN)

Fig. 13 displays comparison of experimental results with model predictions for vertical and horizontal displacements in the R–L section under 20kN compression load for one independent test dataset extracted for each case from bootstrapping. Comparing Figs. 5 and 12 with Fig. 13, some differences between the T–L and R–L sections can be seen. The similarity in magnitudes of vertical displacement u can be expected as most displacement comes from tracheid compression, shear and buckling (Figs. 5a and 13a); however, individual u displacement realisations in the R–L section are more complex than those in the T–L section. As shown in Fig. 4a, the main feature in R–L section is randomly distributed piles of rays spanning their full length and they may explain the high variability observed in a single realisation. Furthermore, u displacement realisations are more far apart than in the T–L section indicating a greater amount of vertical shearing in the R–L section. As for the individual horizontal displacement realisations (v) in the R–L section (Fig. 13c), they are more linear and more spread out than those in the T–L section (Fig. 12a) indicating larger relative displacements (strain) between adjacent vertical columns of points in the R–L section compared to T–L section. In the R–L section, main contributors to horizontal displacement are lignin and rays that could provide a restraining effect. How these contribute to the observed behaviour needs further investigation. The validation R^2 for the two independent test sets (bootstrapped) for u was 0.801 and 0.798, respectively, and for v , 0.803 and 0.796, respectively. Results for the two independent validation specimens were within the CI bounds generated from the models.

4.4 Displacement Profiles in the T–L and R–L Sections (40kN)

This section discusses the influence of structure on the vertical and horizontal displacements when loaded with a 40kN load parallel-to-grain in compression. SNNs were developed for simulating these displacements in both T–L and R–L sec-

tions and they had high accuracy: [T–L: R^2 for the two independent test sets were 0.82 and 0.80, respectively, for vertical displacement and 0.80 and 0.79, respectively, for horizontal displacement; R–L: R^2 for the two independent test sets were 0.806 and 0.799, respectively, for vertical displacement, and 0.802 and 0.798, respectively, for horizontal displacement]. The data for the two validation specimens were within the CI bounds generated from the respective models for both sections. Furthermore, some interesting wood behaviour under high compression load was observed. For the vertical displacement in the T–L section, the relative displacement or vertical shearing across the specimen was much less (curves were more compact) than that for 20kN (Fig. 5a). It indicates that compaction in the structure at 40kN has reduced the relative vertical movement between adjacent vertical lines of points. Noise in each profile also appeared to be smaller at 40kN indicating that the structure has become less heterogeneous with smaller level of noise. Some contributing factors can be ray compaction and/or collapse and tracheid buckling/collapse.

For the horizontal displacement in the T–L section, these displacement profiles were nonlinear as was the case for 20kN (Fig. 12a); however, they are even more compact with less noise compared to 20kN case. This indicates even smaller relative horizontal displacements (strains) between adjacent vertical lines at the higher load. In contrast, in the R–L section, although the higher load had increased the displacements, it had not brought the realisations closer as happened in the T–L section, i.e. realisations were still far apart from each other for both u and v . There was a minor reduction in noise in each profile compared to the 20kN case. Highly prominent vertical shearing and relatively large horizontal strain between adjacent vertical lines were predominant features in the R–L section at both 40kN and 20kN loads.

4.5 Modeling variability in Poisson Ratio in Compression

Poisson ratio is a measure of the tendency of a material to stretch or contract in the perpendicular direction to load. In this study, it is the ratio of

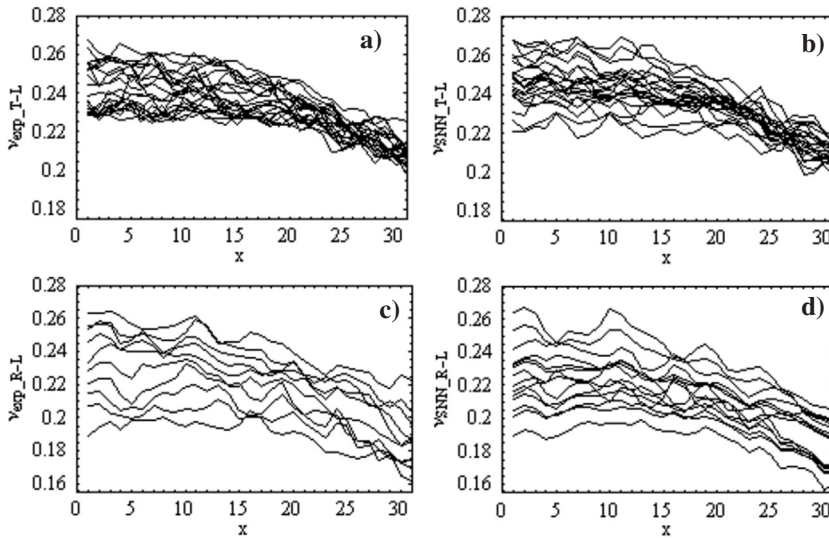


Fig. 14. Comparison of experimental results with model predictions for Poisson ratio (ν) variation along vertical columns of 30 points in the image in the T-L and R-L sections under 20kN compression load: (a) and (c) – experimental Poisson ratio in T-L and R-L sections, respectively; (b) and (d) – SNN predicted Poisson ratio corresponding to the experimental measurements. (Horizontal axis, x , depicts the location of 30 points (10 pixels apart), where displacements were measured. scale: 14.6 pixels/mm for T-L and 14.4 pixels/mm for R-L).

the transverse strain to the longitudinal strain. Poisson ratio is assumed constant for a particular species of wood and its localised variation has not been studied before. In this study, variation of Poisson ratio is examined from experimental data and the ability of stochastic neural networks to capture its intrinsic noise is tested for wood in compression. Fig. 14 compares experimental results with model predictions for Poisson ratio in the T-L and R-L sections under 20kN compression load for one independent test set from bootstrapping for each section.

Fig. 14 shows that Poisson ratio ranges from 0.22 to 0.27 in the T-L section and from 0.19 to 0.26 in the R-L section. These are in general agreement with the limited data from macro-scale measurements reported in the literature (Bodig and Jayne 1982). Poisson ratio in the T-L section is much less variable across the specimen (more compact curves) than that in the R-L section. This can be related to the individual profile characteristics in the two sections. Furthermore, Poisson ratio varies nonlinearly as the distance from the

load to the point increases (i.e. as x increases). Comparison between experimental results (Figs. 14a and c) and SNN predictions (Figs. 14b and d) reveals that the models have captured the variance and noise characteristics of Poisson ratios rather well. The R^2 for the two independent test sets for T-L section was 0.85 and 0.85, respectively, and for R-L section was 0.85 and 0.82, respectively. For each section, data for the two validation specimens were within the CI bounds generated from the respective models. We also analysed Poisson ratio in these two sections under 40kN and found the realisations to be less noisy and more compact with nonlinear trends and values that are lower than those for 20kN. For this case, R^2 for the two independent test sets for the T-L section was 0.843 and 0.82, respectively, and for R-L section was 0.83 and 0.82, respectively. Results for the two validations specimens were within the CI bounds generated from the SNN predicted data.

5 Summary and Conclusions

Stochastic neural networks were developed from experimental displacement fields in the T–L and R–L sections of a specimen for 20kN and 40kN loads using the theory of stochastic processes. The developed stochastic neural networks approximated the experimental vertical and horizontal displacement profiles characterised by variability with high degree of accuracy. Models were successfully validated using two separate validation methods (bootstrapping and Confidence Intervals) with R^2 for validation data ranging from 0.796 to 0.91.

Experiments and models revealed that for 20kN load, the horizontal displacement realisations in the T–L section are less heterogeneous (more compact and smaller strain) compared to those in the R–L section. Magnitude of vertical displacements was similar in the two sections but displacement realisations are far more spread out in the R–L section, indicating higher vertical shearing compared to T–L section. For the 40kN load, both longitudinal and horizontal displacement realisations in the T–L section were more compact (smaller vertical shearing and horizontal strain) than those for the 20kN. Noise of the profiles along the specimen in the T–L section was also much less indicating reduced variability of structure attained through compaction. However, in the R–L section, this phenomenon was not observed and even larger spread between displacement realisations resulted at the 40kN load indicating larger strains (vertical shearing and horizontal strain) compared to 20kN. Why the structure in the T–L section resists vertical shearing and horizontal strains much more at the higher load compared to the lower load, and why the structure in the R–L section undergoes large strains at both lower and higher loads need investigation.

Stochastic neural networks were also developed to model variability in Poisson ratio in the two sections and successfully validated using the two methods mentioned with high accuracy (R^2 ranging from 0.82 to 0.85). The models and experimental results revealed that for 20kN load, Poisson ratio realisations in T–L section are more compact than those in the R–L section and it is

nonlinear in both sections. At 40 kN, Poisson ratio realisations were even far more compact and more nonlinear in the T–L section compared to those under 20kN. However, the R–L section showed a large heterogeneity in Poisson ratios across the specimen for both load levels indicating a complex interaction between tracheids and rays in this section.

The stochastic neural networks were capable of capturing the effects of the heterogeneous structure on wood behaviour. Assuming that the analysed area contains all relevant and essential microstructural details to classify it as a representative area, the outputs generated by the models can be thought of as representing the general character of variation for this wood. Therefore, with further validation, SNN outputs can help simulate behaviour of larger wood specimens with similar general characteristics as an integral part of simulation models where a set of realisations for the structural behaviour of interest can be studied for probabilistic interpretation of the behaviour. The method also has the potential for use in directly assessing variability in large-scale wood members by scanning lightly stressed members and developing SNNs from the data extracted from the images.

References

- Bodig, J. & Jayne, B.A. 1982. Mechanics of wood and wood composites. Van Nostrand Reinhold Company, Inc., USA.
- Choi, D., Thorpe, J.L. & Hanna, R.B. 1991. Image analysis to measure strain in wood and paper. *Wood Science and Technology* 25: 251–262.
- , Thorpe, J.L., Cote Jr., W.A. & Hanna, R.B. 1996. Quantification of compression failure propagation in wood using digital image pattern recognition. *Forest Products Journal* 46(10): 87–93.
- Gilman, I.I. & Skorohod, A.V. 1974. The theory of stochastic processes. Springer-Verlag, Berlin, Germany.
- Jane, F.W. 1956. The structure of wood. A&C. Black Publishers. London.
- Mathematica Version 5.2. 2005. Wolfram Research Inc., USA.

- Nairn, J.A. 2006. Numerical simulations of transverse compression and densification in wood. *Wood and Fiber Science* 38: 576–591.
- Park, J. & Sandberg, I.W. 1991. Universal approximation using radial-basis-function network. *Neural Computation* 3: 246–257.
- Samarasinghe, S. 2006. *Neural networks for applied sciences and engineering: from fundamentals to complex pattern recognition*. CRC Press (Taylor & Francis), Boca Raton, FL, USA.
- & Kulasiri, G.D. 2000a. Displacement fields of wood in tension based on image processing: Part 1. Tension parallel- and perpendicular- to- grain and comparison with isotropic behaviour. *Silva Fennica* 34(3): 251–259.
- & Kulasiri, G.D. 2000b. Displacement fields of wood in tension based on image processing: Part 2. Crack-tip displacement in mode-I and mixed-mode fracture. *Silva Fennica* 34(3): 261–274.
- & Kulasiri, G.D. 2004. Stress intensity factor of wood from crack-tip displacement fields obtained from digital image processing. *Silva Fennica* 38(3): 267–278.
- , Kulasiri, G.D. & Jamieson, T. 2007. Neural networks for predicting fracture toughness of individual wood samples. *Silva Fennica* 41(1):105–122.
- Stelmokas, J.W., Zink, A.G. & Loferski, J.R. 1997. Image correlation analysis of multiple-bolted connections. *Wood and Fiber Science* 29(3): 210–227.
- Turchetti, C. 2004. *Stochastic models of neural networks*. IOS Press, Amsterdam.
- Zink, A.G, Davidson, R.W. & Hanna R.B. 1995. Strain measurement in wood using a digital image correlation technique. *Wood and Fiber Science* 27(4): 346–359.

Total of 16 references